Towards Light Transport Matrix Processing for Transparent Object Inspection

Johannes Meyer
Karlsruhe Institute of Technology KIT
Vision and Fusion Laboratory
Karlsruhe, Germany
https://www.meyer-research.de

Thomas Längle and Jürgen Beyerer
Fraunhofer-Institute of Optronics,
System Technologies and
Image Exploitation IOSB
Karlsruhe, Germany

***Abstract*—Objects made out of transparent materials play important roles in human's everyday life. The majority of applications that employ transparent materials require them to meet high quality standards. Particularly, transparent materials have to be free from so-called scattering defects, e.g., enclosed air bubbles. Common dark field setups can generally be used to automatically test transparent objects for such defects. However, their adaption to the concrete test object on hand often represents a time consuming task. This contribution introduces a method that combines an optical system consisting of a telecentric camera and a spatially programmable area light source with the theory of light transport matrices. Two features are presented that can be extracted out of these matrices and that allow to image scattering defects present in a transparent object without the need of adapting the system to the actual test object. A physically based rendering framework is adequately extended so that light transport matrices can be efficiently approximated for synthetic inspection scenes. By this means, the proposed approach could be successfully evaluated and it could be shown that it even outperforms a conventional visual inspection setup in some situations.**

Keywords*—light transport matrix; machine vision; transparent object inspection; image processing; light field processing

I. Introduction

Transparent materials play an important role in diverse industrial fields. For example, they are employed as windshields of automobiles and aircrafts, they precisely guide laser beams to their intended position in eye surgeries or they are part of high performance optical components. All these example applications clearly point out that transparent materials have to meet high quality requirements.

Typical fabrication defects by which transparent objects can be affected are enclosed absorbing particles, enclosed air bubbles, surface scratches, anomalies with respect to the intended 3D-shape or inhomogeneities of the index of refraction. Depending on the actual application, these defects can have disastrous consequences, which is why a quality control by visual inspection is indispensable. However, since this is a fatiguing task for human workers it is prone to errors and solutions based on automated visual inspection systems for transparent objects have to be found.

There exist automated visual inspection methods for some of the named types of defects [1]–[5]. However, imaging scattering defects, e.g., enclosed air bubbles or surface scratches, still represents a challenging problem. These defects are not causing changes of the transmitted light's intensity but are only manifested in the distribution of the directions of light rays exiting the object under test. Depending on the test object's size and on the wavelength of the employed illumination, different physical effects, e.g., Mie scattering or Rayleigh scattering cause incident light beams to be either widened or scattered [6], [7]. A common approach to image such scattering defects are so-called dark field setups [8]. The constellation of illumination and image acquisition components of such setups ensure, that in the case of a defect-free test object, no (or nearly no) light reaches the employed sensor. On the contrary, if the test object is affected by a scattering defect, the defect results in a scattering of parts of the illuminating light into the sensor and the defect gets visible. Dark field setups all share a notable disadvantage. The arrangement of the setup's sensing and illuminating components with respect to the position and orientation of the test object often have to be determined empirically, what can be costly in terms of time. This is why dark field setups are not suitable for visual inspection applications with a great and varying diversity of test objects.

This paper introduces a novel method capable of imaging scattering defects in transparent objects. The presented approach exploits the directional information of light exiting the test object and does not require a specially adapted arrangement of the illumination sources and image acquisition components with respect to the test object. The method is based on the theory of so-called light transport matrices (LTMs) [9]–[14]. Section II shows the method's optical setup and introduces the definition of a light transport matrix. A physically based renderer is employed to evaluate the proposed method. The respective framework has been extended as shown in Sec. III, so that it allows a comfortable and efficient approximation of the LTMs for the simulated scenes. Section IV introduces two features that can be extracted out of LTMs and that are suitable for the final goal of scattering defect detection. Section V covers the conducted experiments and discusses the results and Sec. VI closes the paper with a summary and an outlook concerning future research topics.

II. Optical setup

The optical setup proposed by this paper is based on a telecentric camera and a spatially programmable area light source. Figure 1 shows the schematic setup of the optical system. The programmable light source could be realized by,

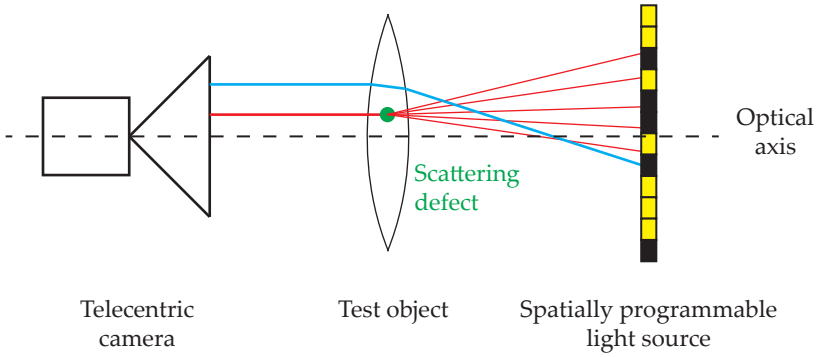

Fig. 1. Optical setup of the proposed approach: a telecentric camera focuses the test object. A spatially programmable area light source illuminates the test object. If a bundle of rays of sight originating from the camera observe a defect-free region of the test object (blue optical path), they only reach a few different pixels of the light source. On the contrary, if the rays of sight pass a scattering material defect (red optical path), they are scattered into multiple directions and reach multiple, spatially spread pixels of the light source.

e.g., a matrix display whose single pixels can be individually turned on and off. A double-convex lens represents the test object in the example shown in Fig. 1.

The telecentric camera captures only light rays that run approximately parallel to the optical axis [8]. If a camera pixel observes a defect-free region of the test object, the respective rays of sight remain bundled while traversing the optical system and reach only a few different pixels of the light source. In contrast, if there is a scattering defect present inside the test object, many light rays originating from different pixels of the light source are scattered into multiple directions. Some of the scattered rays will propagate parallel to the optical axis and will be captured by the telecentric camera. Hence, the signal of a camera pixel observing a scattering defect results from the superposition of light rays coming from multiple different pixels of the programmable light source. The following Sections of this paper show, how these effects can be exploited for imaging scattering defects.

a) Light transport matrix: In the presented optical setup, the signal observed by every camera pixel $\mathbf{k} = (k_m, k_n)^{\mathrm{T}}$ can be influenced by every pixel of the light source $\mathbf{l} = (l_p, l_q)^{\mathrm{T}}$. Hence, for a camera with $M \times N$ pixels and a programmable light source with $P \times Q$ pixels, the complete light transport of the scene can be expressed by means of the so-called light transport matrix

$$\mathbf{T} = \begin{pmatrix} \mathbf{c}(1,1)^{\mathrm{T}} \\ \mathbf{c}(1,2)^{\mathrm{T}} \\ \vdots \\ \mathbf{c}(M,N-1)^{\mathrm{T}} \\ \mathbf{c}(M,N)^{\mathrm{T}} \end{pmatrix}, \tag{1}$$

with the row vectors $\mathbf{c}(m,n)^{\mathrm{T}}$ denoting so-called correspondence vectors [10]. A correspondence vector $\mathbf{c}(m,n) = (c_1(m,n), c_2(m,n), \ldots, c_{PQ-1}(m,n), c_{PQ}(m,n))^{\mathrm{T}}$ contains the components of the PQ light source pixels that result in the signal captured by the camera pixel $(k_m, k_n)^{\mathrm{T}}$. So, every row of $\mathbf{T}$ represents the formation of the signal of the respective camera pixel.

By means of the light transport matrix $\mathbf{T}$ of a certain scene, the camera image $\mathbf{y}$ corresponding to an arbitrary illumination pattern $\mathbf{x}$ of the light source can by calculated by a simple matrix vector multiplication:

$$\mathbf{y} = \mathbf{T}\mathbf{x}\,. \tag{2}$$

The following Section shows, how LTMs can be approximated for simulated scenes by adequately extending an existing rendering framework.

III. Light Transport Matrix Approximation

In order to enable an evaluation of the approach in its early stage, the physically based rendering framework Mitsuba has been employed and adequately extended [15]. Figure 2 shows the schematic concept of the framework. The parts marked in black are the basic core components of Mitsuba. In order to calculate the image of a sensor, e.g., a camera, that observes a scene consisting of different objects and light sources, the following steps are carried out: The framework's main component, the renderer, chooses a sensor sample (pixel of the camera) and an aperture sample (position on the sensor's aperture) following a certain strategy. Based on these samples, the employed sensor component calculates a ray of sight that the renderer traces through the scene until there is no more reflection or the ray has hit a light source. If in the latter case the light source emits light in the direction of the ray of sight, the respective radiance is propagated back to the camera along the optical path in reverse order. During that step, the transported radiance is continuously updated by taking into account the reflectance spectra of all material surfaces that are part of the traversed optical path. Eventually, the final radiance together with the sensor sample are passed to the film component. This component successively aggregates all pairs of sensor samples and radiance values and calculates the final sensor image.

In order to calculate the light transport matrix for a given scene, the Mitsuba rendering framework has been extended by the red components shown in Fig. 2. If a ray of sight hits a pixel $(l_p, l_q)^{\mathrm{T}}$ of a programmable light source, not only the emitted radiance but also the pixel's coordinates will be propagated back. Out of the pairs of sensor samples $\mathbf{k}$ and reached pixels $\mathbf{l}$ of the light source, the renderer successively updates the correspondence vectors $\mathbf{c}$ and finally constructs the light transport matrix $\mathbf{T}$ as shown in Sec. II.

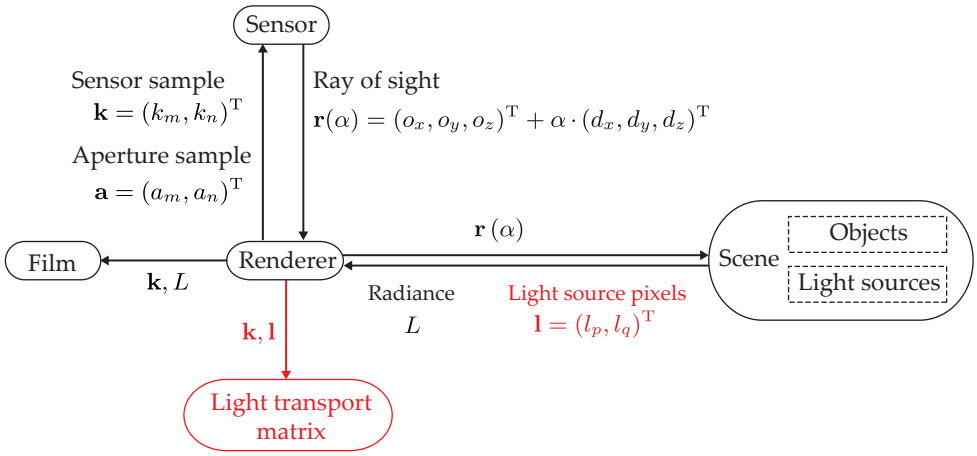

Fig. 2. Schematic concept of the employed rendering framework. The basic components of the Mitsuba renderer are marked in black and the added components are marked in red.

IV. Feature Extraction out of Light Transport Matrices

Based on light transport matrices that were calculated for an inspection setup as shown in Fig. 1, features can be extracted that allow to visualize scattering material defects present in transparent objects. The following two Sections introduce two such features.

A. Feature ScatterCount

As described in Sec. II, scattering defects widen and spread the rays of sight of the telecentric camera, so that they hit multiple pixels of the light source. In other words, rays coming from the illuminating pixels are scattered in such a way, that some of them propagate parallel to the optical axis and are captured by the telecentric camera. Hence, for a camera pixel $(k_m, k_n)^{\mathrm{T}}$, that images a scattering defect, many components of the respective correspondence vector $\mathbf{c}(m,n)$ are greater than zero.

The feature *ScatterCount*

$$sc(m,n) := |\{i \in [1,\ldots,PQ] : \mathbf{c}_i(m,n) \geq 0\}| \tag{3}$$

contains for every camera pixel $(k_m, k_n)^{\mathrm{T}}$ the number of components of $\mathbf{c}(m,n)$ that are greater than zero.

B. Feature ScatterWidth

Besides the *ScatterCount*, i.e., the number of different pixels of the light source that contribute to the signal of a camera pixel, also the maximum distance on the light source, the so-called *ScatterWidth* between the involved pixels conveys useful information. For example, intensely scattering material defects result in a larger area of light source pixels contributing to the signal of the respective camera pixel. The feature *ScatterWidth* is defined as:

$$sw(m,n) := \begin{cases} 0 & , \text{if } \max_{i\in[1,\ldots,PQ]} \mathbf{c}_i(m,n) = 0, \\ \Omega - A & , \text{otherwise}, \end{cases} \tag{4}$$

with

$$A, \Omega \in [1,\ldots,PQ]\,, \tag{5}$$
$$\forall i \in [1,\ldots,A-1] : \mathbf{c}_i(m,n) = 0, \tag{6}$$
$$\forall i \in [\Omega+1,\ldots,PQ] : \mathbf{c}_i(m,n) = 0, \tag{7}$$
$$\mathbf{c}_A(m,n) > 0, \mathbf{c}_\Omega(m,n) > 0\,, \tag{8}$$

so A is the index of the first and Ω the index of the last entry of $\mathbf{c}(m,n)$ that are greater than zero.

V. Experiments

In order to evaluate the proposed method, the inspection setup shown in Fig. 1 has been simulated as virtual scenes using the rendering framework Mitsuba, that has been extended as described in Sec. III. The resolution of the simulated telecentric camera was 100×100 and the resolution of the programmable area light source was 500×500. For every simulated scene the light transport matrix has been approximated and the two features *ScatterCount* and *ScatterWidth* have been extracted for every spatial position. A double-convex lens represented the test object. These kinds of test objects are especially challenging for common inspection setups, since they are imaging optical elements themselves.

Four different instances of the virtual inspection scene have been set up. The first one contains a defect-free test object. In the remaining three instances, the test object is affected by three enclosed air bubbles. The size of the defects is different for every inspection scene and the smallest defect size is equal to half the size of the projection of a camera pixel. The positions of the defects inside the test object are the same for all inspection scenes: one defect is located at the center of the double-convex lens and the other two defects were moved towards the test object's boundary in equidistant steps.

In order to compare the method against an existing approach, additional inspection images of the described scenes were simulated using a conventional inspection system consisting of a telecentric camera and a uniform area illumination [16].

Figure 3 shows an overview of the results of the experiments. The values of the extracted features *ScatterCount*

and *ScatterWidth* are visualized as spatially resolved pseudo color images. The conventional inspection system is capable of imaging all defects of all simulated sizes. However, the images of the smallest defects show only low contrast and are barely visible. Conversely, the two features of the proposed approach visualize even the smallest defects with high contrast, what would be beneficial for a subsequent defect detection. Especially the inspection image resulting from the feature *ScatterWidth* clearly shows the defects. The randomly occurring white dots visible in the images corresponding to the feature *ScatterWidth* are caused by the sampling noise of the rendering framework.

VI. Summary and outlook

This paper shows how an optical system consisting of a telecentric camera and a spatially programmable area light source can be used in concert with methods based on the theory of light transport matrices in order to realize an inspection system capable of visualizing scattering material defects inside transparent objects. It furthermore shows that scattering defects in transparent materials mainly cause changes in the distribution of the directions of incident light rays and they are not manifested in changes of the light's intensity. The light transport matrix of a scene contains all the information about the contribution of each pixel of the light source to the signals captured by the sensor pixels. For the proposed optical system, this information especially contains the direction of the captured light rays.

Two features were introduced that are extracted out of the scene's light transport matrix and that are suitable for visualizing scattering material defects inside transparent objects. A physically based rendering framework has been extended so that it allowed an efficient approximation of light transport matrices for synthetic inspection scenes. By means of the performed experiments it could be shown that the proposed approach is capable of testing transparent objects for scattering defects and that it might even be superior to conventional inspection systems.

As further steps, the authors plan a practical realization of the approach and to conduct real experiments. Therefore, it especially has to be investigated, how the relevant parts of the light transport matrix can be efficiently optically approximated. Furthermore, further features based on the light transport matrices could be defined. For example, the proposed feature *ScatterWidth* does not take the two-dimensional structure of the programmable light source into account in its current state. By exploiting this additional information, the feature could even allow the discrimination of different defect characteristics.

References

[1] M. Hartrumpf and R. Heintz, "Device and method for the classification of transparent components in a material flow," Patent WO 2009/049594 A1, 2009.

[2] M. Hartrumpf, K.-U. Vieth, T. Längle, and G. Struck, "Neues verfahren zur sichtprüfung transparenter materialien," in *Sensorgestützte Sortierung*, 2008, pp. 57–58.

[3] J. Meyer, "Visual inspection of transparent objects – physical basics, existing methods and novel ideas," Karlsruhe Institute of Technology, Tech. Rep. IES-2014-04, 2014.

[4] ——, "Overview on machine vision methods for finding defects in transparent objects," Karlsruhe Institute of Technology, Tech. Rep. IES-2015-08, 2015.

[5] S. Chatterjee, "Determination of refractive index in-homogeneity of transparent, isotropic optical materials," in *Advances in Optical Science and Engineering*. Springer, 2015, pp. 61–66.

[6] C. F. Bohren and D. R. Huffman, *Absorption and Scattering of Light by Small Particles*. Wiley-VCH Verlag GmbH, 2007.

[7] H. van de Hulst, *Light Scattering by Small Particles*, ser. Dover Books on Physics. Dover Publications, 1957.

[8] J. Beyerer, F. P. León, and C. Frese, *Machine Vision: Automated Visual Inspection: Theory, Practice and Applications*. Springer Berlin Heidelberg, 2015.

[9] J. Bai, M. Chandraker, T.-T. Ng, and R. Ramamoorthi, "A dual theory of inverse and forward light transport," in *Computer VisionECCV 2010*. Springer, 2010, pp. 294–307.

[10] M. O'Toole and K. N. Kutulakos, "Optical computing for fast light transport analysis." *ACM Trans. Graph.*, vol. 29, no. 6, p. 164, 2010.

[11] J. Wang, Y. Dong, X. Tong, Z. Lin, and B. Guo, "Kernel Nyström method for light transport," in *ACM Transactions on Graphics (TOG)*, vol. 28. ACM, 2009, p. 29.

[12] M. Chandraker, J. Bai, T.-T. Ng, and R. Ramamoorthi, "On the duality of forward and inverse light transport," *Pattern Analysis and Machine Intelligence, IEEE Transactions on*, vol. 33, no. 10, pp. 2122–2128, 2011.

[13] S. M. Seitz, Y. Matsushita, and K. N. Kutulakos, "A theory of inverse light transport," in *Computer Vision, 2005. ICCV 2005. Tenth IEEE International Conference on*, vol. 2. IEEE, 2005, pp. 1440–1447.

[14] M. O'Toole, J. Mather, and K. Kutulakos, "3d shape and indirect appearance by structured light transport," in *Proceedings of the IEEE Conference on Computer Vision and Pattern Recognition*, 2014, pp. 3246–3253.

[15] W. Jakob, "Mitsuba renderer," 2010, http://www.mitsuba-renderer.org.

[16] J. Meyer, R. Gruna, T. Längle, and J. Beyerer, "Simulation of an inverse schlieren image acquisition system for inspecting transparent objects," *Electronic Imaging*, vol. 2016, no. 19, pp. 1–9, 2016.

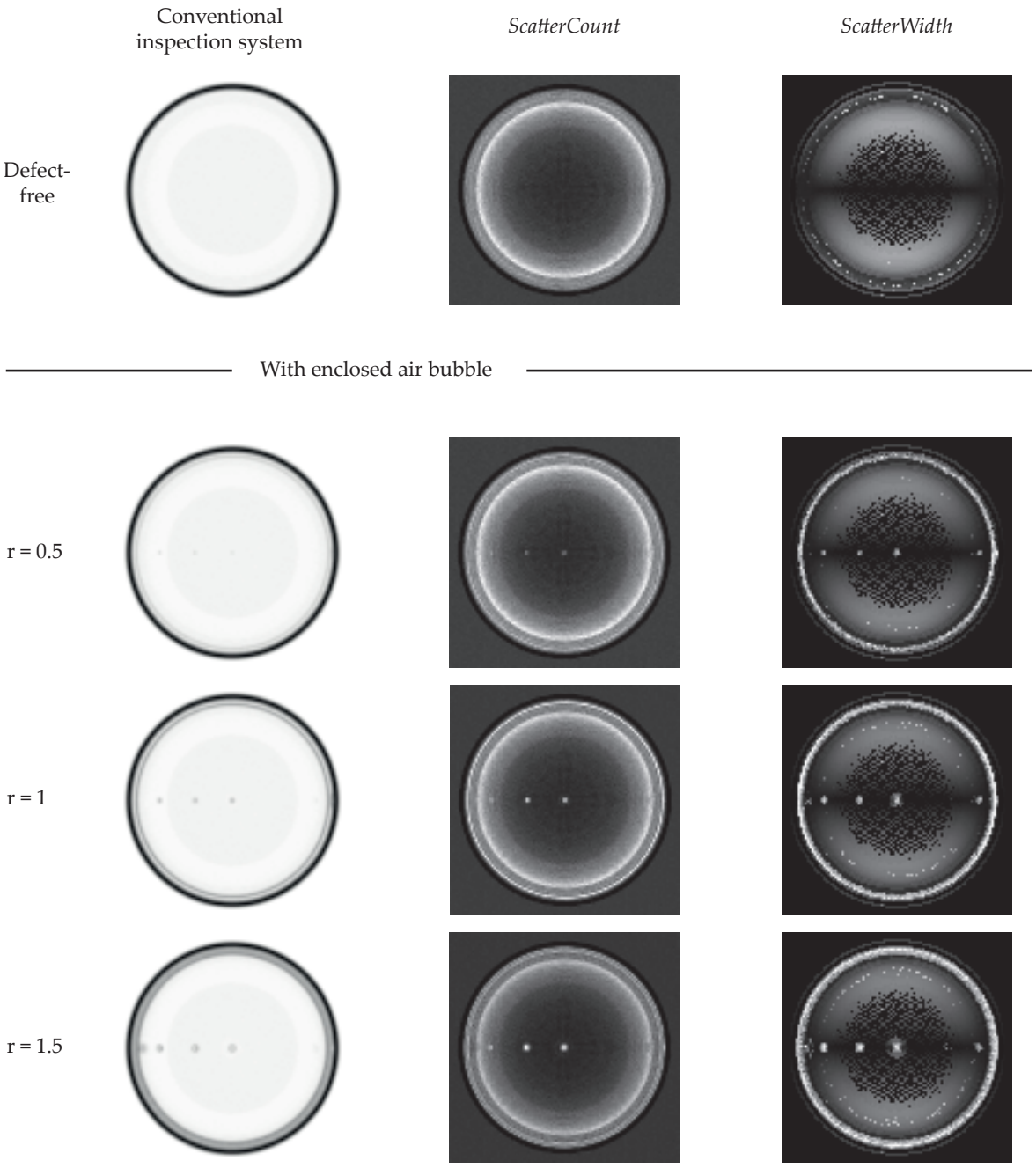

Fig. 3. Simulated inspection images of the conventional inspection system and pseudo color images of the features *ScatterCount* and *ScatterWidth* that are based on the approximated light transport matrices. The size r of the simulated defects denotes a factor with respect to the area of a camera pixel's projection into the scene.